

THE COSMIC NEAR INFRARED BACKGROUND: REMNANT LIGHT FROM EARLY STARS

Elizabeth R. Fernandez and Eiichiro Komatsu

Department of Astronomy, University of Texas at Austin, 1 University Station, C1400,
Austin, TX 78712

beth@astro.as.utexas.edu

ABSTRACT

The redshifted ultraviolet light from early stars at $z = 10$ contributes to the cosmic near infrared background. We present detailed calculations of its spectrum with various assumptions about metallicity and mass spectrum of early stars. We show that if the near infrared background has a stellar origin, metal-free stars are not the only explanation of the excess near infrared background; stars with significant metals ($Z = 1/50$) can produce the same amount of background intensity as the metal-free stars. We quantitatively show that the predicted average intensity at $1.2 \mu\text{m}$ is essentially determined by the efficiency of nuclear burning in stars, which is not very sensitive to metallicity. We predict $I = 1.35 \pm 8 \text{ nW m}^{-2} \text{ sr}^{-1}$, where μ is the mean star formation rate at $z = 7 \pm 15$ (in units of $\text{M}_\odot \text{ yr}^{-1} \text{ Mpc}^{-3}$) for stars more massive than 5 M_\odot . On the other hand, since we have very little knowledge about the form of mass spectrum of early stars, uncertainty in the average intensity due to the mass spectrum could be large. An accurate determination of the near infrared background allows us to probe formation history of early stars, which is difficult to constrain by other means. While the star formation rate at $z = 7 \pm 15$ inferred from the current data is significantly higher than the local rate at $z < 5$, it does not rule out the stellar origin of the cosmic near infrared background.

Subject headings: cosmology: theory | diffuse radiation | infrared: galaxies

1. INTRODUCTION

When and how was the universe reionized? These questions have actively been studied almost purely by theoretical means (see Barkana & Loeb (2001); Bromm & Larson (2004);

Ciardi & Ferrara (2005) for recent reviews), as currently there are only a very few observational probes of the epoch of reionization: the Gunn-Peterson test (Gunn & Peterson 1965; Becker et al. 2001), polarized light of the cosmic microwave background on large angular scales (Zaldarriaga 1997; Kaplinghat et al. 2003), which has been detected by the Wilkinson Microwave Anisotropy Probe (WMAP) (Kogut et al. 2003), and temperature of the intergalactic medium (Hui & Haiman 2003). Over the next decades, we are hoping to detect the first sources of light directly with the next generation of space telescopes, such as the James Webb Space Telescope (JWST). More ambitious are mapping observations and measurements of the power spectrum of fluctuations of the 21-cm line background from neutral hydrogen atoms during reionization (Ciardi & Madau 2003; Furlanetto, Sokasian, & Hernquist 2004) or even prior to reionization (Scott & Rees 1990; Madau, Meiksin, & Rees 1997; Tozzi et al. 2000; Iliev et al. 2002), which offer very powerful probes of detailed history of the cosmic reionization.

It has been pointed out that the mean intensity (Santos, Bromm, & Kamionkowski 2002; Salvaterra & Ferrara 2003; Cooray & Yoshida 2004; Madau & Silk 2005) as well as fluctuations (Migliocchetti, Salvaterra, & Ferrara 2003; Kashlinsky et al. 2004; Cooray et al. 2004) of the near infrared background potentially offer yet another window to the epoch of reionization. The logic is very simple: suppose that most of reionization occurred at, say, $z = 9$. The ultraviolet photons ($\sim 1000\text{\AA}$) produced at $z = 9$ during reionization will then be redshifted to the near infrared regime ($\sim 1\text{ \mu m}$). In other words, a fraction of the near infrared background (whether or not observable) must come from the epoch of reionization, and there is no question about the existence of the signal. (Of course the existence of the signal does not immediately imply that the signal is actually significant.) It is therefore extremely important to understand the near infrared background in the context of redshifted UV photons and examine to what extent it is relevant to and useful for understanding the physics of cosmic reionization.

Has it been detected? All of the theoretical proposals were essentially motivated by the current measurements of the near infrared background, which suggests the existence of an isotropic background after subtraction of the zodiacal emission (Dwek & Arendt 1998; Gorjian, Wright & Chary 2000; Wright & Reese 2000; Wright 2001; Cambresy et al. 2001; Matsumoto et al. 2005). Since the zodiacal emission is 3 times as large as the inferred isotropic component, one should generally be careful when interpreting the data. Although the inferred background is isotropic at the first order, significant fluctuations still remain at the level of $I = I_0 / 1 = 4$ (Kashlinsky & Odenwald 2000; Kashlinsky et al. 2002; Matsumoto et al. 2005), which requires further explanations. The most intriguing feature of the current observational data is that the inferred background seems too large to be accounted for by the integrated light from galaxies (see Figure 12 of Matsumoto et al. (2005) and references

therein for the compilation of the galactic contribution). It is thus tempting to speculate that the bulk of the near infrared background (aside from the zodiacal light) actually comes from stellar sources at the epoch of reionization.

In this paper, we carefully examine the near infrared background from early stars. While our approach is similar to that of Santos, Bromm, & Kamionkowski (2002), which has been adopted by most of the subsequent work, our goal is to (1) simplify physics and improve calculations, (2) explore different metallicity and initial mass spectra, (3) understand robustness of theoretical predictions, and (4) provide a simple relation between the cosmic near infrared background and star formation rate. The focus of this paper is the mean intensity: we will discuss fluctuations in the forthcoming paper (Fernandez et al., in preparation). This paper is organized as follows. In $\S 2$, we develop the basic formalism and summarize relevant emission processes such as stellar emission and reprocessed light, the latter including Lyman-, two-photon, free-free and free-bound emission. In $\S 3$, we examine energy spectra of various emission processes from early stars. In particular we explore differences in the energy spectrum between various assumptions about metallicity and initial mass spectrum of early stars. In $\S 4$, we calculate the spectrum of the cosmic near infrared background. In $\S 5$, we compare the prediction to the current observational data and discuss implications for the star formation rate at $z = 7 - 15$. In $\S 6$ we discuss the other constraints from a collapse fraction of dark matter halos as well as from metal enrichment in the intergalactic medium. We conclude in $\S 7$.

2. STELLAR EMISSION AND REPROCESSED LIGHT

2.1. Basic Formalism

We calculate the background intensity, I , as (Peacock 1999)

$$I = \frac{c}{4} \int_0^z \frac{dz p([1+z]; z)}{H(z)(1+z)}; \quad (1)$$

where ν is an observed frequency (which is in the near infrared band: for $\nu = 3 - 1 \text{ m}$, say, $\nu = 100 - 300 \text{ THz}$ or $h = 0.414 - 1.24 \text{ eV}$), $H(z)$ is the expansion rate at redshift z ($dt/dz = H(z)(1+z)^{-1}$), and $p(\nu; z)$ is the volume emissivity in units of energy per unit time, unit frequency and unit comoving volume. There are several contributions to the emissivity. One is the continuum emission from stars themselves, p_{cont} , which is nearly a black body spectrum, and the others are reprocessed light of ionizing radiation: a star ionizes neutral gas in its neighborhood and a series of recombination lines, p^{line} , emerge. The ionized gas (or nebula) also emits free-free and free-bound continuum emission, p^{cont} ,

as well as two-photon emission, p^2 . In Appendix A, we derive the formula for the volume emissivity as [Eq. (A 9)]

$$p(z) = \underline{\lambda}(z)c^2 \quad h_i; \quad (2)$$

where

$$h_i = \frac{1}{m} \int_0^Z dm m f(m) \frac{\overline{L}(m)}{m c^2} \frac{h_i^{\#}}{m}; \quad (3)$$

and $f(m)$ is a mass spectrum (specified later in § 3.1; for the precise definition, see Appendix A), and m is the mean stellar mass [Eq. (A 5)]. It is important to note that this formula has been derived assuming that the stellar main-sequence lifetime, $\langle m \rangle$, is shorter than the Hubble time, and corrected for dead stars which do not contribute to the volume emissivity. Here, $\overline{L}(m)$ is a time-averaged luminosity in frequency interval $[m, m + dm]$ for a radiative process of λ , and h_i is the key dimensionless quantity which represents a ratio of the mass-weighted average¹ of total radiative energy (including stellar emission and reprocessed light) to the stellar rest mass energy, in unit frequency interval. In other words, h_i represents the mass-weighted mean radiative efficiency of stars. This formulation is useful as one can immediately see that each contribution is simply given by the star formation rate (which depends on z) and a typical radiative efficiency (which does not depend on z). While $\underline{\lambda}$ is very uncertain and will be constrained by a comparison to the observational data, one can calculate h_i robustly for a given population of stars using simple physical arguments. It will be shown in the subsequent sections that h_i is always of order 10^{-3} , which can be understood on simple energetics. Initially, energy must be generated by nuclear burning in stars. While the rest mass energy of $1 M_\odot$ is as big as 1.8×10^{51} erg, only a fraction will go into radiative energy. For example, in the Sun only 0.07% of the rest mass energy is converted to radiative energy over its main-sequence lifetime. The nuclear burning efficiency² depends on stellar mass only weakly at large masses. Our detailed calculations below confirm this simple argument, and thus the uncertainty in the predicted amplitude of radiative efficiency is small for a given mass spectrum of stars.

Using the expected radiative efficiency of stars, we obtain

$$I = 13.1 \text{ nW m}^{-2} \text{ sr}^{-1} \int_0^Z \frac{dy}{y^2 E(y)} \frac{\underline{\lambda}(y)}{M \text{ yr}^{-1} \text{ Mpc}^{-3}} \times \frac{(y)h_i(y)}{10^{-3}}; \quad (4)$$

¹Throughout this paper, we shall use h_i to denote the mass-weighted average.

²By 'nuclear burning efficiency', we mean the bolometric energy of stellar emission before absorption per stellar rest mass energy, $\overline{L}_{bol} = m c^2$.

where $y = 1 + z$ and

$$E(y) = \frac{p}{h} \frac{1}{y^3 + \frac{m}{0.14} h^2}, \quad 11.83 \quad \frac{m}{0.14} h^2 \quad \frac{y}{10} \quad ; \quad (5)$$

for the redshift range of interest. Thus, without any detailed calculations, one can show that the cosmic near infrared background from early stars at $z = 10$ should be approximately given by $I = 10 \text{ nW m}^{-2} \text{ sr}^{-1}$ where I is in units of $M \text{ yr}^{-1} \text{ Mpc}^{-3}$.

2.2. Stellar Contribution

To simplify calculations, we assume that the stellar spectrum is a black body with the Lyman continuum photons completely absorbed:

$$\bar{L}(m) = \begin{cases} 4 \frac{R^2}{h} B[T_{\text{eff}}(m)]; & h < 13.6 \text{ eV} \\ 0; & h \geq 13.6 \text{ eV} \end{cases} \quad (6)$$

where R is a stellar radius and T_{eff} is the effective temperature, and $B[T_{\text{eff}}(m)]$ is a black body spectrum given by

$$B[T_{\text{eff}}(m)] = \frac{2h^3 c^2}{\exp(h/kT) - 1}; \quad (7)$$

Note that the stellar spectrum (before absorption) above 13.6 eV (which determines the number of hydrogen-ionizing photons) is significantly different from a black body; thus, we do not use a black-body spectrum to calculate the number of ionizing photons, but use more detailed calculations by Schaefer (2002) (see x 3.2). The stellar spectrum just below 13.6 eV is also different from a black body because of a cluster of absorption lines of Lyman series; however, we ignore this effect and keep our calculations as simple as possible. (One can always use a more precise stellar spectrum for a better accuracy.)

2.3. Free-free and Free-bound Contribution

The free-free and free-bound continuum luminosity is given by

$$\bar{L}^{\text{cont}}(m) = \frac{\bar{Q}_H(m)}{n_e n_p B}; \quad (8)$$

where \bar{Q}_H is a time-averaged production rate of hydrogen ionizing photons (the average number of ionizing photons produced per unit time), n_e and n_p are the number density of

electrons and protons, respectively, B is the case-B recombination coefficient for hydrogen (Eq. [5-14] of Spitzer (1978) with $n = 2$ and $Z = 1$) given by

$$B = \frac{2.06 \cdot 10^{11}}{T_g^{1/2}} \cdot \chi_2(T_g) \text{ cm}^3 \text{ s}^{-1}; \quad (9)$$

and $\chi_2(T_g)$ is a dimensionless function of temperature tabulated in Table 5.2 of Spitzer (1978). Here, T_g denotes gas temperature in units of Kelvin. In principle, to calculate T_g one has to equate the energy gain and loss to find out equilibrium temperature. While T_g varies depending on stellar temperature (or hardness of a stellar spectrum which determines photo-heating), we shall assume $T_g = 20000$ K regardless of the stellar temperature, which should be a good approximation for our purposes. For this temperature we find $\chi_2(T_g = 20000 \text{ K}) \approx 1$.

The quantity $\overline{Q}_H(m) = (n_e n_p B)$ is the volume of the Stromgren sphere (see text below Eq. [12]), and " is the total volume emissivity including free-free and free-bound emission (Eq. [6.22] of Dopita & Sutherland (2002)):

$$" = 4 \cdot n_e n_p \cdot c \frac{e^{h/kT_g}}{T_g^{1/2}} \text{ erg cm}^{-3} \text{ s}^{-1} \text{ Hz}^{-1}; \quad (10)$$

where " is the continuum emission coefficient including free-free and free-bound emission:

$$" = f_k \overline{g}_{ff} + \sum_{n=2}^{\infty} \frac{x_n e^{x_n}}{n} g_{fb}(n); \quad (11)$$

where $x_n = RY = (kT_g n^2)$, \overline{g}_{ff} and $g_{fb}(n)$ are the Gaunt factors for free-free (which is thermally averaged) and free-bound emission, respectively, and f_k is the collection of physical constants which has a numerical value of $5.44 \cdot 10^{-39}$ in cgs units. Note that we have ignored the helium contribution and assumed complete ionization for computing ". As a free-bound transition to $n = 1$ will not be considered in the case-B recombination, the summation is taken from $n = 2$. (This is because all photons that recombine directly to $n = 1$ are strongly absorbed by neighboring hydrogen atoms and immediately ionize them.) We then obtain

$$\overline{L}^{\text{cont}}(m) = 3.32 \cdot 10^{32} \text{ erg s}^{-1} \text{ Hz}^{-1} \cdot \frac{\overline{Q}_H(m)}{10^{49} \text{ s}^{-1}} \cdot \overline{g}_{ff} + \frac{RY}{kT_g} \sum_{n=2}^{\infty} \frac{e^{RY/(kT_g n^2)}}{n^3} g_{fb}(n) \cdot \chi_2(T_g) e^{h/kT_g}; \quad (12)$$

The continuum luminosity does not depend on the number density of electrons or protons. This is an immediate consequence of the Stromgren sphere: while the higher number density implies the larger emissivity, it also implies the larger recombination rate and the smaller ionized region. These two effects cancel out exactly, making luminosity independent of the number density. Of course, this approximation breaks down in the intergalactic medium.

(outside of halos) in which ionization fronts do not fill the Stromgren sphere (Shapiro & Girioux 1987). Our calculation assuming the Stromgren sphere is accurate if the bulk of luminosity comes from nebulae around stars inside the host halos, while it should give a robust upper limit on free-free and free-bound luminosity otherwise.

Finally, we need to compute the Gaunt factors. For the parameter space we are interested in,

$$u \quad \frac{h(1+z)}{kT_g} = O(10) \frac{1+z}{10}; \quad (13)$$

$$2 \quad \frac{Ry}{kT_g} = O(10); \quad (14)$$

both Gaunt factors are approximately constant and given by (Kazanas & Latter 1961)

$$\bar{g}_{ff} \approx 1.1; \quad (15)$$

$$g_{fb}(n) \approx 1.05; \quad (16)$$

which are accurate to within 10%.

2.4. Line Contribution

The line luminosity is given by

$$\bar{L}^{\text{line}}(m) = \sum_i^X h_i(\lambda_i) n_i(m); \quad (17)$$

where $h_i(\lambda_i)$ is the line profile and n_i is a photon production rate at a line i . Since the intergalactic medium is optically thick to the Lyman continuum photons before the end of reionization, every single hydrogen-ionizing photon will be absorbed and converted to line emission; thus, the line contribution should be proportional to a production rate of hydrogen-ionizing photons, \bar{Q}_H , as

$$\bar{n}_i(m) = f_i \bar{Q}_H(m); \quad (18)$$

where f_i is a fraction of ionizing photons which are converted to a line i .

Which lines are important to the near infrared background? The Lyman series photons are in right bands; however, they are strongly absorbed and eventually converted to other lines. One exception is the Lyman- α photons: while they are also strongly absorbed, they are re-emitted back again in Lyman- β . Therefore the net effect is that the Lyman- α photons

are not destroyed (in the absence of dust) but merely scattered. Loeb & Rybicki (1999) have shown that as the universe expands the Lyman- α photons are eventually "redshifted out" of scattering and escape freely. The Balmer series photons (and others) have too low an energy to be relevant to the near infrared background (a direct recombination to $n = 2$ results in a line at 3.4 eV or 3648 Å, which will be redshifted to > 3 m and is thus irrelevant). Therefore, we consider only Lyman- α photons:

$$\overline{L}^{\text{line}}(m) = f_{Ly} h_{Ly} (1 - \overline{Q}_H(m)) \cdot 4.51 \cdot 10^{32} \text{ erg s}^{-1} \text{ Hz}^{-1} \frac{\overline{Q}_H(m)}{10^{49} \text{ s}^{-1}} \text{ Ly} (1 - \text{Ly}); \quad (19)$$

where $h_{Ly} = 10.2 \text{ eV}$, $f_{Ly} = 0.64$, and $\text{Ly} = 2465 \text{ THz}$. Note that $f_{Ly} = 0.64$ was derived as follows: every hydrogen-ionizing photon results in a $n = 2 \rightarrow 1$ transition. (This is because every electron that goes directly to the ground state from $n = 3$ emits Lyman-series photons which are strongly absorbed, creating another excited atom, and this process repeats until all electrons end up in $n = 2$ state.) About 2/3 of the time a $n = 2 \rightarrow 1$ transition creates a Lyman- α photon via $2p \rightarrow 1s$ transition and about 1/3 of the time it emits continuum emission via 2-photon decay of $2s \rightarrow 1s$. The precise value of f_{Ly} depends slightly on the temperature of gas, and for a gas at 20,000 K the value of f_{Ly} is 0.64 (Spitzer 1978). Finally, we ignore helium recombination lines as their flux is at most 6% of the hydrogen-ionizing flux even from metal-free stars (see Table 1 and 4 of Schaerer (2002)). As for a line profile, we take it to be a delta function:

$$(1 - \text{Ly}) = \delta(1 - \text{Ly}); \quad (20)$$

This is an excellent approximation as we are interested in the background intensity which is integrated over a broad range of redshifts. If we are, on the other hand, interested in a spectrum of individual objects with fine spectral resolution, more accurate calculations are required (Loeb & Rybicki 1999). We have confirmed validity of our approximation by comparing the resulting spectrum with and without the exact line profile taken into account.

It should be emphasized that the escape fraction, a fraction of ionizing photons escaping from nebula, does not alter luminosity of Lyman- α very much. This is because all of the ionizing photons will eventually be converted to Lyman- α photons which, in turn, will escape freely via the cosmological redshift. Therefore, our prediction is free from uncertainty in the escape fraction. In other words, we do not care where those Lyman- α photons come from as far as the mean intensity is concerned³. If most of the ionizing photons escape from nebulae, Lyman- α photons should come from the intergalactic medium (but not too far away from

³However, the escape fraction should affect fluctuations as it changes morphology of the ionized region.

nebulae; otherwise, the Lyman-alpha signal would be spread over a large frequency range and the signal would be suppressed). If none of the ionizing photons escape, Lyman-alpha photons should come from nebulae. In both cases, the resulting flux in Lyman-alpha should be about the same.

2.5. Two-photon Emission

Luminosity of 2-photon emission is given by

$$\overline{L}^2 (m) = \frac{2h}{ly} (1 - f_{ly}) P(=ly) \overline{Q}_H (m) \\ = 4.24 \cdot 10^{32} \text{ erg s}^{-1} \text{ Hz}^{-1} \cdot \frac{\overline{Q}_H (m)}{10^{49} \text{ s}^{-1}} \cdot \frac{P(=ly)}{ly} = 2; \quad (21)$$

where $P(y)dy$ is the normalized probability per 2-photon decay of getting one photon in the range $dy = dy = ly$. This formula is easily understood: again, every single ionizing photon results in a $n = 2 \rightarrow 1$ transition, and $1 - f_{ly} = 1/3$ (more precisely 0.36 for $T_g = 20,000 \text{ K}$) of time it emits 2 photons via 2-photon decay. (Therefore there is a factor of 2 multiplying h .) We have fitted the data given in Table 4 of Brown & Mathews (1970) to obtain⁴

$$P(y) = 1.307 - 2.627(y - 0.5)^3 + 2.563(y - 0.5)^4 - 51.69(y - 0.5)^6; \quad (22)$$

Note that $P(y)$ is normalized such that $\int_0^1 P(y)dy = 1$. (This fitting formula gives $\int_0^1 P(y)dy = 1.0047$.)

3. ENERGY BUDGET

3.1. Initial Mass Spectrum

In order to calculate a typical spectrum of radiative efficiency, h (Eq. [3]), one needs to specify the mass spectrum of stars, $f(m)$, which determines the mean stellar mass of star formation. (For the precise definition of $f(m)$, see Appendix A.) This is important because, depending on which mass is the most typical one, hardness of the emerging stellar spectrum changes significantly. (Hardness affects a ratio of energy in Lyman-alpha to that in stellar continuum.) Unfortunately, since we have very little knowledge about the form of

⁴Brown & Mathews (1970) tabulate $g(y) = 2hyP(y)$, where $h = 6.626 \cdot 10^{27} \text{ erg Hz}^{-1}$ is Planck's constant.

$f(m)$ for early stars, we are not able to estimate the error associated with changing $f(m)$. While we try to explore a range of models for $f(m)$, one should keep in mind that this is not exhaustive.

We use three different mass spectra: (a) Salpeter (Salpeter 1955):

$$f(m) / m^{-2.35}; \quad (23)$$

and (b) Larson (Larson 1998):

$$f(m) / m^{-1} \frac{m}{m_c}^{1.35}; \quad (24)$$

which matches Salpeter's in the limit of $m_c \rightarrow 0$, and one can explore a variety of models by changing one parameter, m_c . We shall assume $m_c = 50 M_\odot$. Finally, (c) a top-heavy spectrum:

$$\begin{aligned} f(m) / m^{-1}; & 100 < m < 500 M_\odot \\ 0; & \text{otherwise} \end{aligned} \quad (25)$$

which might be possible for the primordial metal-free stars (Bromm & Larson 2004). (Note that $m f(m)$ is flat for $100 < m < 500 M_\odot$.) The normalizations are given by

$$\int_{m_1}^{m_2} dm f(m) = 1; \quad (26)$$

The choice of the mass range is somewhat arbitrary. Throughout this paper, we shall assume $m_1 = 5 M_\odot$ and $m_2 = 150 M_\odot$ for the Salpeter and Larson mass spectra, whereas $m_1 = 100 M_\odot$ and $m_2 = 500 M_\odot$ for the top-heavy spectrum. (We shall explain the reason for $m_1 = 5 M_\odot$ later in § 4.2.) The mean stellar masses (Eq. A5) are 13.6, 27.4, and 248.5 M_\odot for the Salpeter, Larson, and top-heavy spectrum, respectively.

3.2. Metallicity

The next ingredients are the stellar luminosity-mass relation, $\overline{L}(m)$, the ionizing flux-mass relation, $\overline{Q}_H(m)$, the stellar lifetime-mass relation, $\tau(m)$, and the effective temperature-mass relation, $T_{\text{eff}}(m)$. Since these relations mainly depend on metallicity, we explore two cases: (1) metal-free ($Z = 0$) stars, and (2) metal-poor ($Z = 1/50$) stars. Although one might argue that $Z = 1/50$ is not very "metal-poor", we use this metallicity merely as an upper limit. The predicted energy spectrum for other metallicity ($0 < Z < 1/50$) should lie between these two examples.

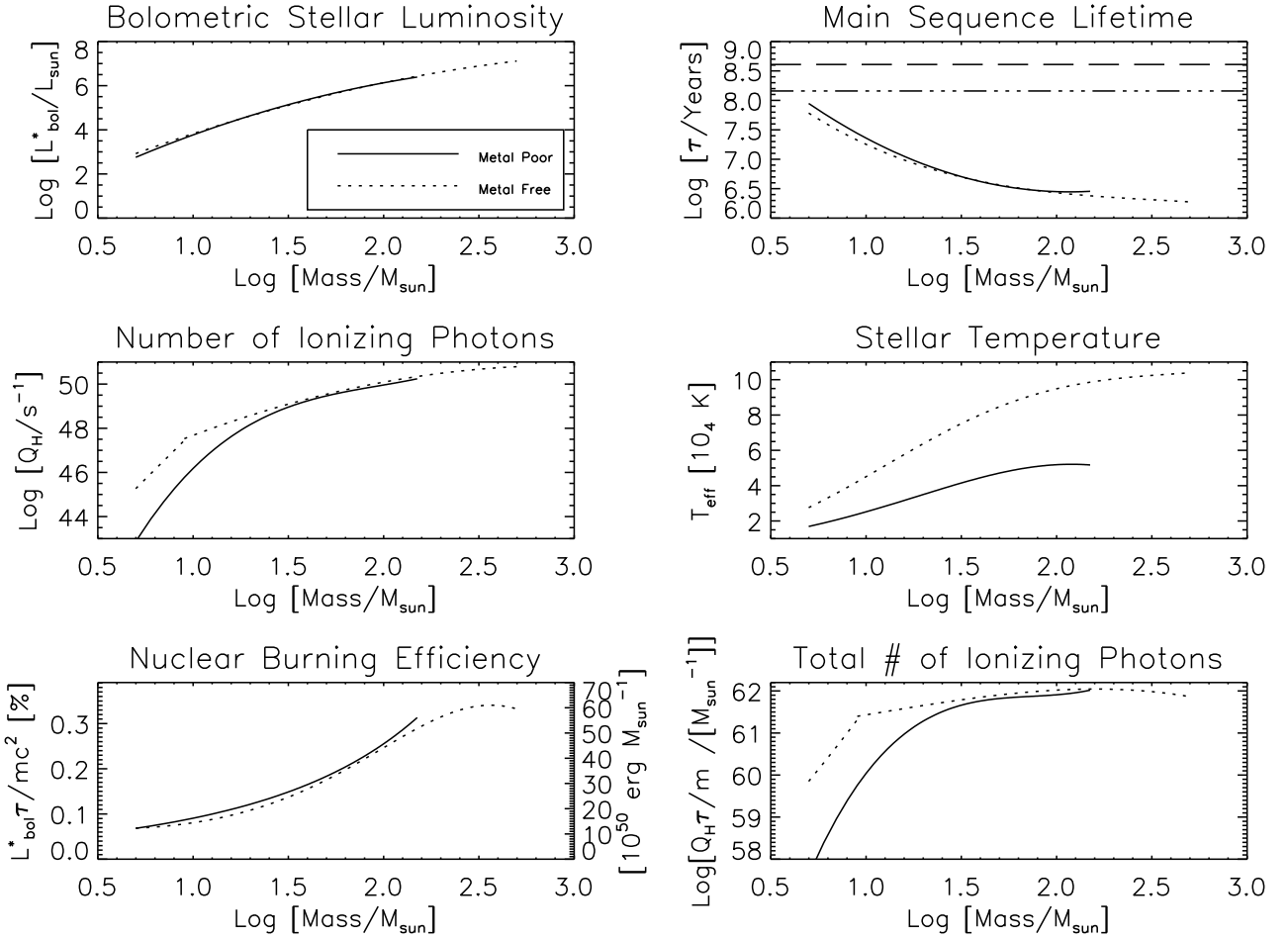


Fig. 1. Stellar properties. (Top-left) The stellar bolometric luminosity, L_{bol} ; (Top-right) the stellar main-sequence lifetime, τ ; (Middle-left) the number of hydrogen-ionizing photons emitted per unit time, Q_{H} ; (Middle-right) the stellar effective temperature, T_{eff} ; (Bottom-left) nuclear burning efficiency, with the axis on the right showing bolometric radiative energy per stellar mass over the main sequence lifetime; and (Bottom-right) the total number of hydrogen-ionizing photons per unit stellar mass, for different stellar metallicities. In the top-right panel, the dashed and dotted horizontal lines show the age of the universe at $z=7$ and 15 , respectively.

3.2.1. Metal-free Stars

Schaerer (2002) has calculated emission properties of metal-free stars. We use his fitting formulas for $\overline{Q}_H (m)$ and (m) over $m = 5 - 500 M_\odot$ (Table 6 of Schaerer (2002)):

$$\log_{10} \overline{Q}_H = s^1 = \begin{cases} 43.61 + 4.90x & 0.83x^2 & 9 & 500 M_\odot; \\ 39.29 + 8.55x & & 5 & 9 M_\odot; \end{cases} \quad (27)$$

$$\log_{10} [= \text{yr}] = 9.785 - 3.759x + 1.413x^2 - 0.186x^3; \quad (28)$$

where $x = \log_{10} (m/M_\odot)$. We calculate the stellar radius as

$$4 \pi R^2 (m) = \frac{L_{\text{bol}} (m)}{T_{\text{eff}}^4 (m)}; \quad (29)$$

where $= 5.67 \times 10^5 \text{ erg s}^{-1} \text{ cm}^{-2} \text{ K}^{-4}$ is the Stephan-Boltzmann constant. The bolometric stellar luminosity before absorption, L_{bol} , and the effective temperature, T_{eff} , are given in Table 3 of Schaerer (2002). These were used to obtain fitting formulas for T_{eff} and L_{bol} , which are good for masses anywhere from $5 - 1000 M_\odot$:

$$\log_{10} [L_{\text{bol}} = L] = 0.4568 + 3.897x - 0.5297x^2 \quad (30)$$

$$\log_{10} [T_{\text{eff}} = K] = 3.639 + 1.501x - 0.5561x^2 + 0.07005x^3 \quad (31)$$

Note that L_{bol} and T_{eff} were calculated for the zero-age main sequence stars, whereas \overline{Q}_H has been averaged over the main-sequence lifetime. Strictly speaking, the former quantities should have also been averaged over the stellar lifetime; however, we shall ignore such a subtlety and use the zero-age values as tabulated in Schaerer (2002).

3.2.2. Metal-poor Stars

For stars with $Z = 1/50$, we use the fitting formula for $\overline{Q}_H (m)$ given in Table 6 of Schaerer (2002), and we fitted the data given in Table 45 of Schaller et al. (1992) for (m) :

$$\log_{10} \overline{Q}_H = s^1 = 27.80 + 30.68x - 14.80x^2 + 2.50x^3; \quad (32)$$

$$\log_{10} [= \text{yr}] = 9.87 - 3.31x + 0.80x^2; \quad (33)$$

where $x = \log_{10} (m/M_\odot)$. The formula for stellar lifetimes is good for masses in the range of $5 - 150 M_\odot$. While the formula for ionizing photons is good from $7 - 150 M_\odot$, we shall extrapolate it down to $5 M_\odot$. We calculate the stellar radius (Eq. 29) using $L_{\text{bol}} (m)$ and

T_{eff} (M) given in Table 1 (22 of Schaller et al. (1992)). The fitting formulas were thus obtained as

$$\log_{10} [L_{\text{bol}} = L] = 0.1530 + 4.728x - 0.8195x^2 + 0.01287x^3; \quad (34)$$

$$\log_{10} [T_{\text{eff}} = K] = 3.7487 + 0.7269x - 0.02720x^2 - 0.04736x^3; \quad (35)$$

Again, L_{bol} and T_{eff} were calculated for the zero-age main sequence stars, whereas \bar{Q}_H has been averaged over the main-sequence lifetime.

3.2.3. Stellar Properties

Figure 1 shows the bolometric stellar luminosity before absorption, L_{bol} (top-left panel), the main-sequence lifetime, τ (top-right), the number of hydrogen-ionizing photons per second, \bar{Q}_H (middle-left), and the stellar effective temperature, T_{eff} (middle-right), for $Z = 0$ (labeled as "metal-free") and $Z = 1=50$ ("metal-poor"). The bolometric luminosity is very similar for metal-free and metal-poor stars at the same stellar mass down to $10 M_\odot$ (Tumlinson & Shull 2000), and is almost identical for more massive stars ($> 100 M_\odot$) (Bromm, Kudritzki & Loeb 2001). Since metal-free stars had to begin their nuclear burning via the p-p chain, which is less efficient than the CNO cycle because of weak interactions, the temperature of metal-free stars must be maintained higher than that of metal-poor stars to prevent gravitational collapse (Tumlinson & Shull 2000). Since the luminosity is similar, this property makes the size of metal-free stars smaller and the main-sequence lifetime slightly shorter than those of metal-poor stars. On the other hand, metal-free stars produce more hydrogen-ionizing photons than metal-poor stars, particularly for $M > 30 M_\odot$, owing to their higher temperature (the spectrum is harder).

The bottom panels of Figure 1 show quantities more relevant to the radiative efficiency, η . The first panel shows the ratio of the stellar bolometric energy to the rest mass energy. This figure shows that for $M > 10 - 100 M_\odot$ anywhere from 0.1 to 0.3% of the rest mass energy of the star goes into radiative energy via nuclear fusion; thus, this quantity represents a "nuclear burning efficiency" of stars. The metal-poor stars radiate slightly more energy over their lifetime than the metal-free stars, as they live slightly longer and the bolometric luminosity is about the same. On the right, the total number of ionizing photons per unit stellar mass, $\bar{Q}_H = \eta$, is shown. The metal-poor stars emit significantly less ionizing photons for $M > 30 M_\odot$: this property becomes important when we interpret the predicted spectrum of the near infrared background.

3.3. Energy Spectrum

Using these fitting formulas and the initial mass spectra, we calculate a spectrum of radiative efficiency averaged over the mass spectrum for $m = m_1 - m_2$ (Eq. [3]). Figure 2 shows h_i for the stellar (Eq. [6]), nebular continuum (free-free and free-bound) (Eq. [12]), Lyman- (Eq. [19]), and two-photon (Eq. [21]) emission. The nebular continuum dominates at low energy, while the stellar, Lyman- and two-photon emission dominate at high energy, as expected from their spectral shape. Since metallicity changes hardness of the stellar spectrum, it affects a ratio of energy in Lyman- and two-photon emission to stellar emission energy: the harder the spectrum is, the more the ionizing photons are emitted, and thus the more the Lyman- and two-photon emission emerge⁵. This explains why the metal-free stars have much more energy in Lyman- and two-photon emission than in stellar emission. On the other hand, the metal-poor stars have more energy in stellar emission. For the same reason, heavier mass spectra tend to produce more energy in Lyman- and two-photon emission than in stellar emission. In both cases, however, the total radiative efficiency is about the same: $h_i \approx 10^3$. This is merely an approximate conservation of energy: initially all the energy was generated by nuclear burning in stars. The generated energy is then radiated or reprocessed, but the sum should be more or less the same as the input energy. (Of course conservation cannot be exact because we have ignored other emission processes such as Balmer lines, helium or metal lines, etc. If the H II region expands, additional energy would be lost to expansion.) This property makes the prediction of the near infrared background very robust, up to an unknown star formation rate, $\dot{\rho}$, which will be constrained by a comparison to the observational data.

4. SPECTRUM OF THE NEAR INFRARED BACKGROUND

4.1. Dependence on Metallicity and Initial Mass Spectrum

By integrating the volume emissivity over redshift, we obtain the background intensity spectrum of the near infrared from early stars (Eq. [4]). To do this, however, one needs to specify the evolution of star formation rate over time, $\dot{\rho}(z)$, which is unknown. Therefore, for simplicity, we shall assume that the star formation rate is constant over time, at least

⁵ However, this is not always the case. The bottom-right panel of Figure 1 shows that metal-poor stars actually emit many ionizing photons per stellar mass as metal-free stars form $\approx 30 M_\odot$; thus, if the mean stellar mass of metal-poor stars were $\approx 30 M_\odot$, metal-poor stars would result in as many Lyman- photons as metal-free stars.

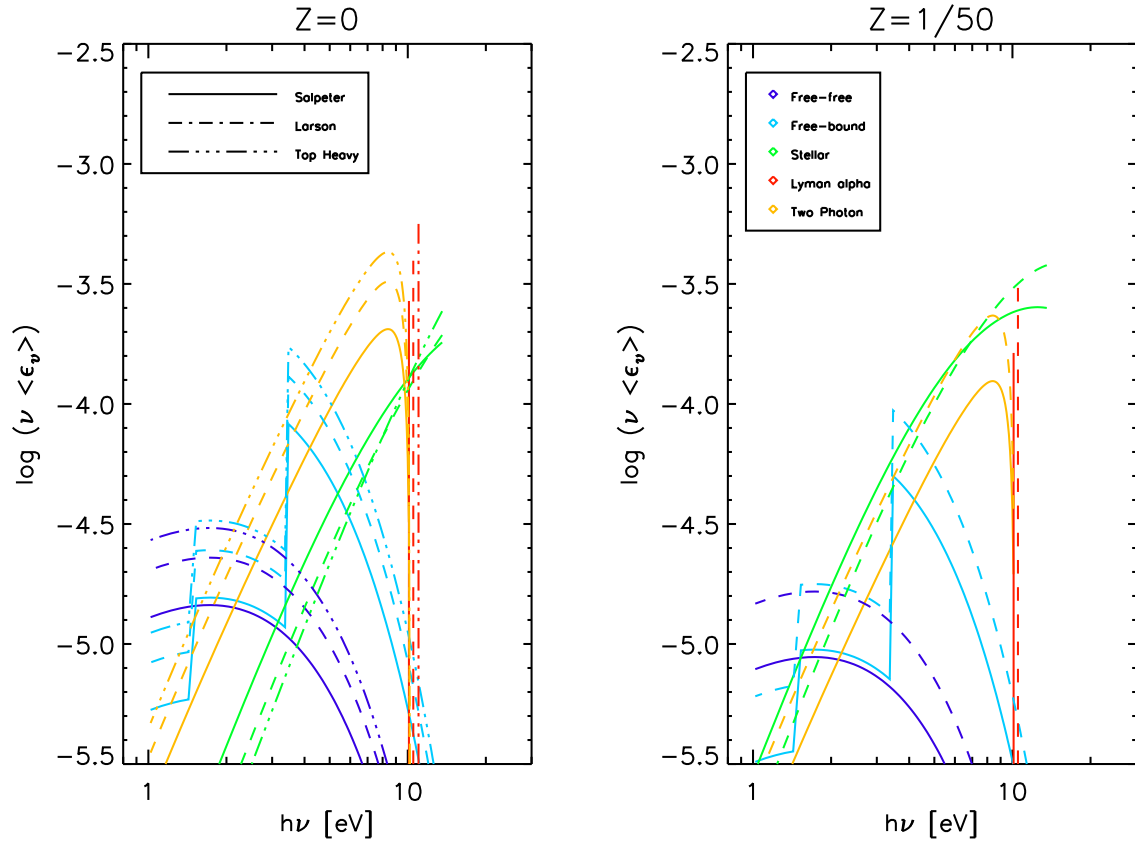


Fig. 2.1 Spectrum of radiative efficiency, $\log(\langle \nu < \epsilon_\nu \rangle)$, for different metallicities: $Z = 0$ (left) and $Z = 1/50$ (right). The radiative efficiency is defined as a fraction of the stellar rest mass energy that goes into free-free (the lowest purple lines), free-bound (the "saw-shaped" cyan lines), stellar black-body (green), two-photon emission (orange) or Lyman-alpha (the vertical red lines) emission. The solid, dot-dashed, and triple-dot-dashed lines show the Salpeter (Eq. [23]), Larson (Eq. [24]), and top-heavy (Eq. [25]) initial mass spectra, respectively.

for the redshift range of interest. In other words, we calculate the intensity spectrum for a given "time-averaged" star formation rate. Figure 3 and 4 show $I =$ for stars in three redshift ranges, $z = 7 - 15, 15 - 30$, and $7 - 30$. These figures clearly show that the intensity at $1 - 2 \text{ m}$ is almost entirely determined by the contribution at $z = 7 - 15$. (Note that Lyman- α lines at $z = 7 - 15$ are redshifted to $1 - 2 \text{ m}$.) Therefore, the spectrum of the near infrared background at $1 - 2 \text{ m}$ constrains the star formation rate at $z = 7 - 15$!

Table 1 summarizes values of $I =$ averaged over $1 - 2 \text{ m}$. Within $1 - 2 \text{ m}$, the intensity is dominated by Lyman- α emission. For metalpoor stars, there is also a significant contribution from stars themselves, which brings the overall intensity for metalpoor and metalfree stars to be about the same. This seems striking, but is merely a consequence of an approximate energy conservation, as discussed in $\times 3^6$. Therefore, the predicted intensity is not sensitive to stellar metallicity.

As for dependence on the initial mass spectrum, $f(m)$, heavier mass spectra tend to give higher background intensities. Energetics implies that dependence of $I =$ on metallicity or $f(m)$ should be essentially given by that of the nuclear burning efficiency averaged over a population of stars. The last column of Table 1 shows the mass-weighted mean nuclear burning efficiency, $h_{\text{L,bol}} = (m c^2) i$, which is tightly correlated with the total signal. Therefore, one can explore dependence of the near infrared background on these parameters by simply calculating the nuclear burning efficiency dependence on these parameters. In order to illustrate how nuclear burning efficiency changes with respect to the shape of $f(m)$, we show the efficiency for various values of the lower mass limit, m_1 , and the critical mass, m_c , for the Salpeter (Eq. [23]) and Larson (Eq. [24]) initial mass spectra in Figure 5. The average nuclear burning efficiency for $m_1 > 20 M_\odot$ depends very weakly on m_c , while the dependence is stronger for $m_1 < 20 M_\odot$. Dependence on m_1 also becomes stronger as m_1 becomes smaller. Overall, for Larson's mass spectrum, different m_1 and m_c may change the predicted intensity by a factor of a few, but not much more. However, one should keep in mind that other forms of $f(m)$ that we have not explored here might change the predicted intensity by a larger factor.

4.2. Comparison with Previous Work

Santos, Broom, & Kamionkowski (2002) calculated the near infrared background from metal-free stars, assuming that all early stars contributing to the background light have

⁶We thank Paul R. Shapiro for pointing out potential importance of metalpoor stars for the near infrared background.

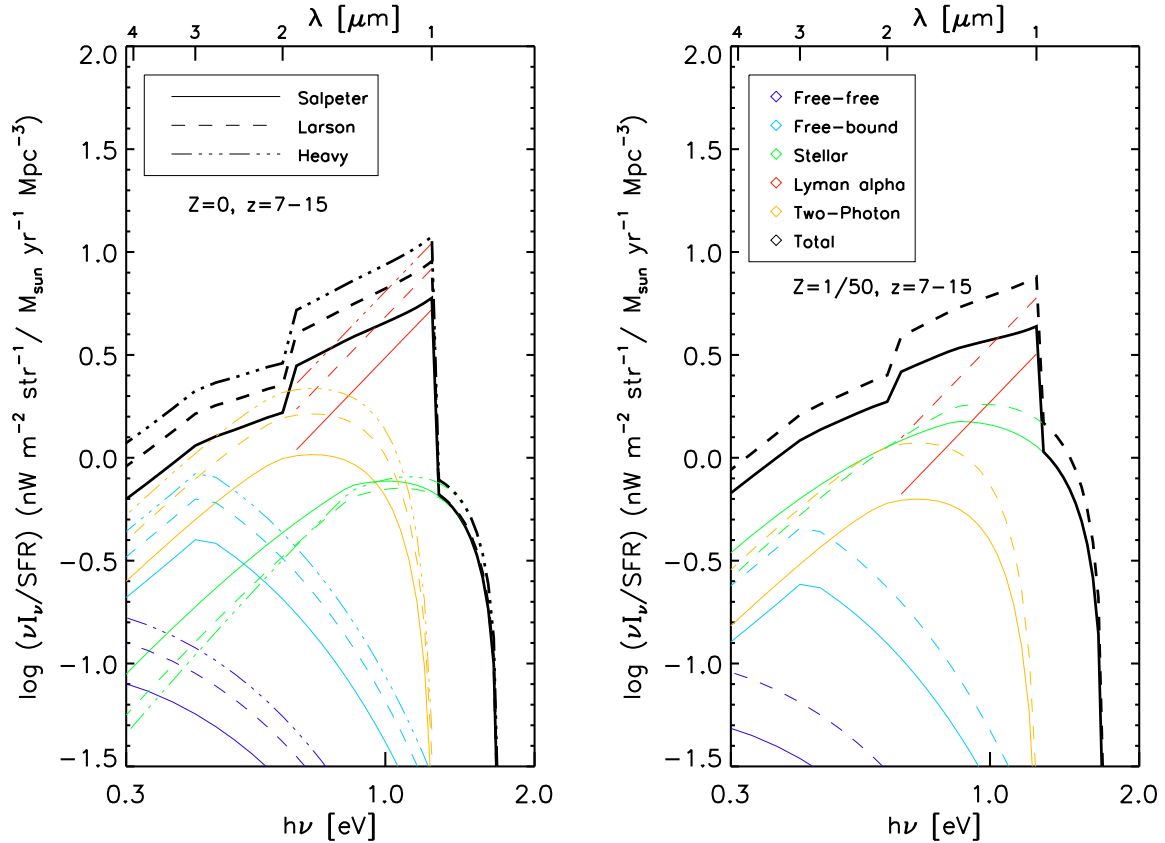


Fig. 3.] Spectrum of the near infrared background, $I = \text{...}$, for star formation from $z = 7$ to 15 with various assumptions about metallicity and initial mass spectrum. ($\text{\textbackslash SFR}$ " in the axis label denotes ...) The left panel shows the metal-free case ($Z = 0$), while the right panel shows the metal-poor case ($Z = 1=50$). The solid, dashed, and triple-dotted-dashed lines represent the Salpeter, Larson, and top-heavy mass spectrum, respectively. The thick black lines show the total spectrum, while the thin purple, cyan, green, red and orange lines show individual contribution from free-free, free-bound, stellar, Lyman- α and two-photon emission, respectively.

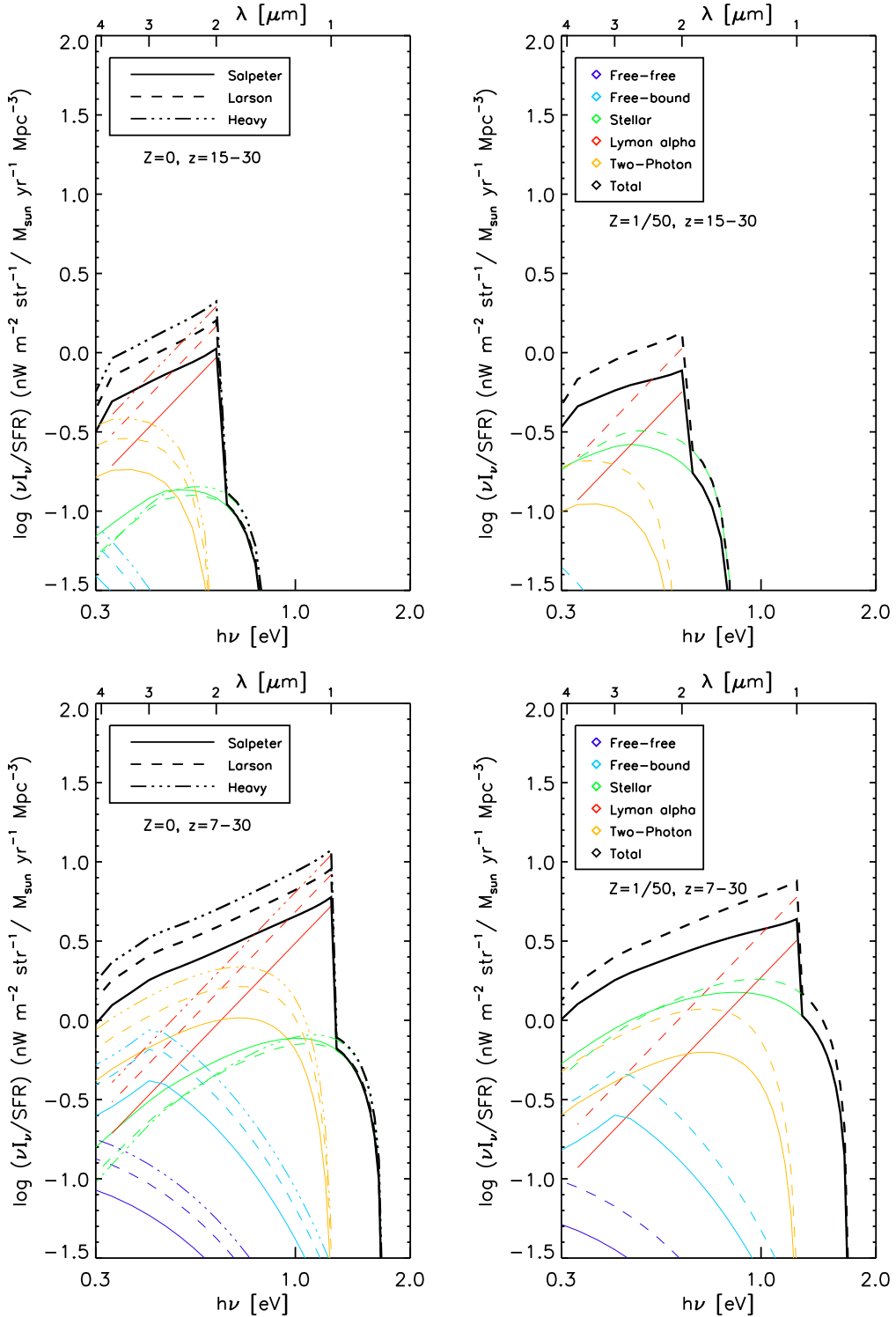


Fig. 4. The same as Figure 3 for $z = 15-30$ (top) and $z = 7-30$ (bottom).

Metallicity	IMF	Stellar	Free-free	Free-bound	Luminance	Two-photon	Total	$10^3 h \frac{L_{bol}}{M_{\odot}}$
Metal-Poor	Salpeter	1.35	0.00595	0.0461	1.64	0.415	3.46	1.35
	Larson	1.62	0.0112	0.0865	3.08	0.778	5.58	1.84
Metal-Free	Salpeter	0.678	0.00979	0.0759	2.71	0.683	4.15	1.25
	Larson	0.605	0.0154	0.120	4.27	1.08	6.08	1.73
	Top Heavy	0.663	0.0205	0.159	5.67	1.43	7.95	3.23

Table 1: Values of $I = \langle \dots \rangle$ averaged over $1 \leq m \leq 2 M_{\odot}$ in units of $\text{nW m}^{-2} \text{sr}^{-1} = \text{M}_{\odot} \text{yr}^{-1} \text{Mpc}^{-3}$ from each radiative process. Here $\langle \dots \rangle$ is the mean star formation rate for $m > 5 M_{\odot}$ at $z = 7, 15$, and $\text{hL}_{\text{bol}} = \langle m \dot{c} \rangle$ is the mass-weighted mean nuclear burning efficiency of stars.

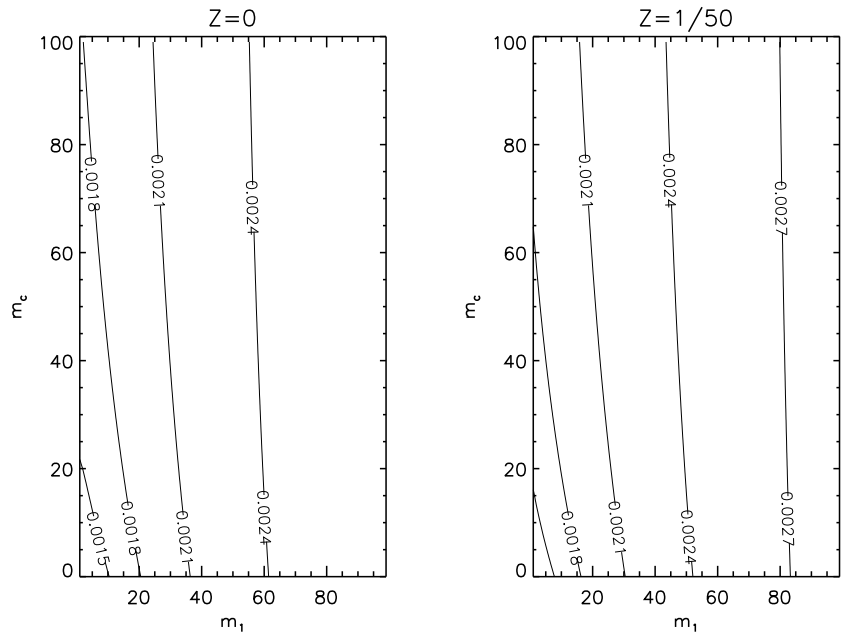


Fig. 5.1 Mass-weighted mean nuclear burning efficiency, $hL_{\text{bol}} = (m^2/c)i$, resulting from varying the initial mass spectrum. Each contour shows a different nuclear burning efficiency, and m_1 and m_c are the lower mass limit of star formation and the critical mass in Larson's mass spectrum (Eq. [24]), respectively.

$m = 1000 M_{\odot}$ (i.e., $f(m) = \frac{D}{m} (m - 1000 M_{\odot})$). While the stellar, Lyman- α , and free-free emission were included in their calculations, the two-photon and free-bound emission were ignored. As we have shown in Figure 3, the contribution from free-bound transition to $n = 2$ is much larger than the free-free contribution, and the contribution from two-photon emission is as important as that from stellar emission; thus, they must be included.

Salvaterra & Ferrara (2003) assumed metal-free stars but explored different initial mass spectra, varying m_c of Larson's spectrum. There is a subtle but important difference between their approach and our approach. When they modeled the volume emissivity, they did not allow for the faster rate of death of higher mass stars. In other words, their formula for the volume emissivity implicitly assumed that stars lived longer than the Hubble time. We find that the volume emissivity that is not corrected for dead stars (Eq. A 6]) agrees with their formula (Eq. [5] and [12] in Salvaterra & Ferrara (2003)). This assumption leads to an overestimation of contributions from higher mass stars which live much shorter than the Hubble time. The physical reason is because higher mass stars live shorter and die sooner, and therefore there are fewer massive stars around to emit energy at a given z . By properly taking into account the faster rate of death of stars, we have obtained the correct formula (Eq. [A 9]) which explicitly depends on the stellar main-sequence lifetime. On the other hand, if stars live longer than or comparable to the Hubble time, then our approximation breaks down and one should do the integral in equation (A 8). This is precisely why we have restricted our attention only to fairly massive stars, $m > 5 M_\odot$, for which the age of the universe is definitely longer than the main-sequence lifetime at redshifts of interest.

5. IMPLICATIONS FOR THE COSMIC STAR FORMATION RATE

5.1. Star Formation Rate at $z = 7 - 15$

Comparing the predicted values of $I = \dots$ (Table 1) to the measured data, we can constrain the star formation rate \dots . The near infrared background has been determined with various satellites, such as the *Dust Infrared Radiation Background Experiment* (DIRBE) on the *Cosmic Background Explorer* (Boggess et al. 1992) and the *Near Infrared Spectrometer* (NIRS) on the *InfraRed Telescope in Space* (IRTS) (Matsumoto et al. 2005). Table 2 summarizes the observational data. A significant uncertainty exists in the observational data, largely because of uncertainty in subtraction of the zodiacal emission. A large difference between Wright (2001) and Cambresy et al. (2001), which have used the same data (DIRBE), is entirely due to difference in the zodiacal light models. One may summarize the current measurement of the cosmic near infrared background as $2 - 50 \text{ nW m}^{-2} \text{ sr}^{-1}$ in $1\{2 \text{ m}$, which includes the 1- lower bound of the lowest measurement and the 1- upper bound of the highest measurement. Taking into account a scatter in theoretical predictions due to different assumptions about metallicity and initial mass spectrum (see Table 1 and 3), we obtain $0.3 - 15 \text{ M}^{-1} \text{ yr}^{-1} \text{ Mpc}^{-3}$ at $z = 7 - 15$. (Note that the error bar is not dominated by theory but by observational errors.) What does this imply?

Instrument	I		Reference
DIRBE	14.6	12.4	Wright (2001)
	30.9	12.8	Cambrésy et al. (2001)
NIRS	41.6	9.7	Matsumoto et al. (2005)

Table 2: Observational data of I averaged over $1 \text{--} 2 \text{ m}$ in units of $\text{nW m}^{-2} \text{sr}^{-1}$. Note that zodiacal emission, emission of foreground stars, and emission from galaxies have been subtracted. For DIRBE, the straight average of J- and K-band data (minus $10 \text{ nW m}^{-2} \text{sr}^{-1}$ which is contributed by galaxies) is quoted, and the error is estimated as $\sqrt{(\frac{1}{J} + \frac{1}{K})} = 2$. For NIRS, the straight average of 9 measurements from $1.43 \text{ to } 2.24 \text{ m}$ is quoted, and the error is estimated similarly as $\sqrt{\frac{9}{i=1} \frac{1}{i}} = 9$. Statistical errors are negligible compared to the systematic errors in subtraction of the zodiacal emission. For details, see Matsumoto et al. (2005).

5.2. Stellar Mass Density Constraints on fronts Cosmic Baryon Density

One must always make sure that the stellar mass density inferred from star formation rate does not exceed the cosmic mean baryon density. Using the formula derived in Appendix B, we obtain a ratio of cumulative mass density (which is not corrected for dead stars) of stars formed at $7 < z < 15$ to the cosmic mean baryon density as

$$\frac{\text{cum } (7 < z < 15)}{b_0} = 0.0747 \frac{0.024}{b h^2} \frac{0.14}{m h^2} \frac{1^{1/2}}{M \text{ yr}^{-1} \text{ Mpc}^{-3}} ; \quad (36)$$

where $b_0 = 2.775 \cdot 10^{11} (b h^2) \text{ M}^{-1} \text{ Mpc}^{-3}$ is the present-day mean baryon density. (Note that cum denotes comoving mass density.) It follows from this equation that the inferred lower limit to the star formation rate, $\dot{M} > 0.3 \text{ M}^{-1} \text{ yr}^{-1} \text{ Mpc}^{-3}$, requires that more than 2% of baryons in the universe should have been converted into stars. Madau & Silk (2005) argue that "this is energetically and astrophysically daunting". It would be daunting, if the stars that were responsible for producing the near infrared background lived longer than the age of the universe, and more than 2% of baryons had remained locked up in the stars. However, it is certain that stars lived much shorter than the age of the universe (see the top-right panel of Figure 1), and the stellar mass density must be corrected for dead stars; thus, the actual amount of baryons locked up in stars at any given time between $z = 7$ and 15 should be less than that is given by equation (36). We derive the stellar mass density corrected for dead stars in Appendix B 2, which shows that the correct answer should lie between equation (36) and equation (36) divided by the mean number of generations of stars, N_{gen} , given by

$$N_{\text{gen}} = \frac{t(7 < z < 15)}{\int_{m_1}^{m_2} dm f(m) / (m)} ; \quad (37)$$

Metallicity	IMF	— (Lower limit)	— (Upper limit)	N_{gen}	= b [%] (Lower limit)	= b [%] (Upper limit)
Metal-Poor	Salpeter	0.58	15	7.3	0.59	15.3
	Larson	0.36	9.0	12.8	0.21	5.3
Metal-Free	Salpeter	0.48	12	10.0	0.36	9.0
	Larson	0.33	8.2	16.7	0.15	3.7
	Top Heavy	0.25	6.3	120	0.016	0.39

Table 3: Implications of the current lower and upper limits to the cosmic near infrared background data, $I = 2 \text{ nW m}^{-2} \text{ sr}^{-1}$ and $I = 50 \text{ nW m}^{-2} \text{ sr}^{-1}$, for formation of early stars with $m > 5 \text{ M}_\odot$ during $z = 7 - 15$. The third and forth columns show the lower and upper limits, respectively, to the star formation rate in units of $\text{M}_\odot \text{ yr}^{-1} \text{ Mpc}^{-3}$, the fifth column shows the mean number of generations of stars (Eq. B7]), and the sixth and seventh columns shows the lower and upper limits, respectively, to a ratio of stellar density to the mean cosmic baryon density in percentage.

and $t(7 < z < 15) = 266$ million years is the cosmic time elapsed during $z = 7 - 15$. Table 3 tabulates N_{gen} for various assumptions about metallicity and initial mass spectrum. From this we conclude that, to explain the cosmic near infrared background by early generations of stars, 0.016{15% of baryons need to be processed in stars at a given time between $z = 7$ and 15. If we take the lower 1- limit, only 0.016{0.59% of baryons need to be processed in stars (depending on metallicity and mass spectrum); this is not a daunting requirement and does not exclude the stellar origin of the cosmic near infrared background⁷.

5.3. Comparison with Low Redshift Data

How does the inferred star formation rate at $z = 7 - 15$ compare to the low- z rate? Figure 6 compares the cosmic star formation rate at $z < 5$ (Gabasch et al. 2004)⁸ to that constrained by the near infrared background. While uncertainty due to subtraction of the

⁷Our argument so far has implicitly assumed that all of baryonic gas in the previous generation of stars is returned to the intergalactic medium and recycled in the subsequent generation of stars. In reality, however, only a fraction of gas would be returned (and the rest of gas would be locked up in compact remnants such as black holes); thus, the real requirement would be somewhat larger than 0.016{0.59%.

⁸The rate at $z < 5$ has been shifted upward by 0.35 dex to correct for dust extinction. More recent determination of the star formation rate by Drory et al. (2005) agrees very well with Gabasch et al. (2004).

zodiacal light is large, it is quite clear that the star formation rate at $z = 7 - 15$ required to account for the cosmic near infrared background data is much higher than that at $z < 5$ by more than an order of magnitude.

It must be emphasized, however, that Figure 6 is potentially misleading: as we have already discussed, the star formation rate inferred from the near infrared background is only for stars more massive than $5 M_{\odot}$. On the other hand, the low- z data are primarily dominated by low mass stars; thus, Figure 6 might be comparing apples and oranges. As such low mass stars do not contribute to the near infrared background, it is not possible to infer their formation rate directly. One may still estimate it by extrapolating the initial mass spectrum down to lower masses, and by doing so the total star formation rate at $z = 7 - 15$ should rise. In other words, the constraint shown in Figure 6 should be taken as a lower bound. Also, dust extinction (which we have ignored), if any, would make the required star formation rate rise even higher.

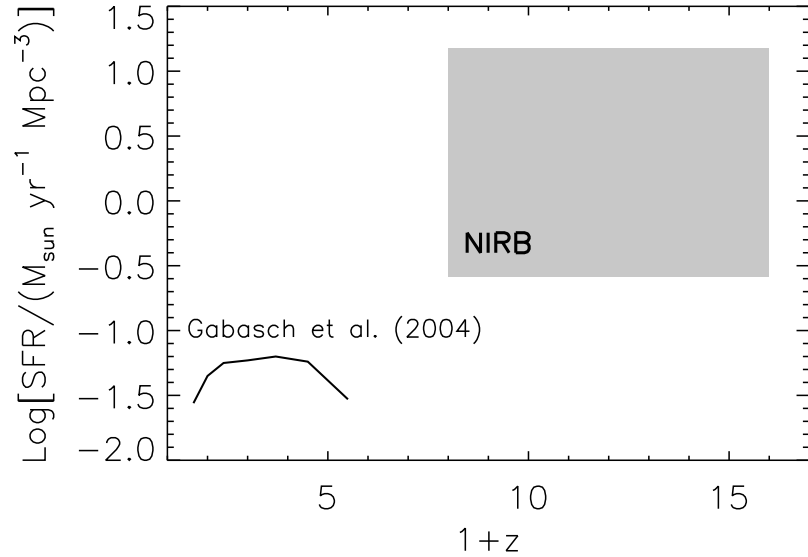


Fig. 6.1 Cosmic star formation rate. The shaded region shows the star formation rate for $m > 5 M_{\odot}$ constrained by the current data of the cosmic near infrared background, $I = 2 - 50 \text{ nW m}^2 \text{ sr}^{-1}$, in $1\{2 \text{ m}$. The solid line shows the star formation rate at $z < 5$ (Gabasch et al. 2004). Note that the shaded region should be taken as a lower bound. (See discussion in § 5.3).

6. REMARKS ON OTHER CONSTRAINTS

6.1. Amplitude of Matter Fluctuations at Small Scales

In the previous work on the near infrared background from early stars (Santos, Bromm, & Kamionkowski 2002; Salvaterra & Ferrara 2003; Madau & Silk 2005), it was concluded that a substantial fraction of collapsed baryons in the universe must have been converted into stars. In § 5.2 we have considered a fraction of all baryons in the universe that was locked up in stars at a given z , and now it is natural for us to ask how many baryons collapsed in dark matter halos were converted into stars. Of course, this fraction, η , which is sometimes called the "star formation efficiency", must not exceed unity.

In Appendix C, we derive an analytical model for the cosmic star formation rate (Eq. [C 6]) which has often been used in the literature:

$$\eta(z) \approx 0.536 M_{\odot} \text{ pc}^{-3} \text{ yr}^{-1} \frac{1+z}{10}^{3/2} \eta_{\text{min}}(z) e^{-\eta_{\text{min}}^2(z)/2}; \quad (38)$$

where

$$\eta_{\text{min}}(z) \approx \frac{1.68(1+z)}{M_{\text{min}}(z)}; \quad (39)$$

and M_{min} is the present-day rms amplitude of mass fluctuations given by

$$\eta^2(M_{\text{min}}) = \int_0^{z=1} \frac{k^2 dk}{2^2} P(k) \frac{3j_1(kR_M)}{kR_M}^2; \quad (40)$$

Here, $P(k)$ is the linear power spectrum of density fluctuations at present, $j_1(x) = \sin(x)/x = x^2 \cos(x)/x$ is the spherical Bessel function of order 1, R_M is a radius defined by $M_{\text{min}} = (4\pi/3)\rho_0 R_M^3$, and $M_{\text{min}}(z)$ is the minimum mass of dark matter halos which can host star formation. For illustration purposes, let us assume that star formation occurs when cooling via atomic hydrogen becomes efficient, $M_{\text{min}}(z) > M_{\text{min}}(z) \approx 10^8 M_{\odot}$ [$(1+z)=10$] $^{3/2}$ (Barkana & Loeb 2001). This mass scale roughly corresponds to the wavenumber of $k = 1/R_M$ & $36.8[(1+z)=10]^{1/2} M_{\odot} \text{ pc}^{-1}$.

By comparing this analytical model to the observational data, one can constrain and/or $M_{\text{min}}(z)$. The usual approach is to constrain $M_{\text{min}}(z)$ by fitting $P(k)$ extrapolated from $k = 1 M_{\odot} \text{ pc}^{-1}$ (which corresponds to $M_{\text{min}} \approx 5 \times 10^2 M_{\odot}$) down to much smaller scales, $k \approx 36.8[(1+z)=10]^{1/2} M_{\odot} \text{ pc}^{-1}$, for which we do not have any direct observational constraints yet. This is potentially a dangerous approach. Equation (38) implies that $\eta(z)$ is exponentially sensitive to $M_{\text{min}}(z)$, and a slight increase in $M_{\text{min}}(z)$ may substantially reduce $\eta(z)$ for a given $M_{\text{min}}(z)$, and thus one must not ignore the fact that we do not

know the precise value of $M_{\text{min}}(z)$] without relying on extrapolations of $P(k)$ by a factor of more than 40 in k . Therefore, the stellar origin of the near infrared background cannot be ruled out on the basis of until we understand the amplitude of matter fluctuations on small scales. One may reverse the argument: it might be possible to explore the small-scale fluctuations by using the near infrared background, for a given star formation efficiency.

6.2. Metal Enrichment

Since formation of massive stars must be accompanied by death of the same stars within the Hubble time, which often injects metals to the intergalactic medium, abundance of metals at high redshifts offers an additional constraint to the formation history of early stars. This point has been investigated by Santos, Bromm, & Kamionkowski (2002) and Salvaterra & Ferrara (2003) in the context of the near infrared background. The general results obtained by these studies suggest that the universe would be over-enriched unless the mixing of metals was highly inhomogeneous or most of the metals were locked up in compact remnants such as black holes, the importance of latter largely depending on the initial mass spectrum. While metal enrichment is certainly a powerful tool to test the stellar origin of the near infrared background, given a large uncertainty in the initial mass spectrum and theory of mixing of metals in the intergalactic medium, we conclude that the current observations do not rule out the stellar origin.

7. CONCLUSIONS

We have presented detailed theoretical calculations of the intensity of the cosmic near infrared background from early stars. We have shown that the intensity is essentially determined by the mass-weighted mean nuclear burning energy of stars (for a given mass spectrum of early stars) and the cosmic star formation rate. The prediction is not sensitive to stellar metallicity (Table 1), while uncertainty from the initial mass spectrum could be large, as we have very little knowledge about the form of mass spectrum for early stars. The measured intensity at $1 < z < 2$ can be used to infer the cosmic star formation rate at $7 < z < 15$, which is difficult to constrain by other means. Although the current data are quite uncertain due to subtraction of the zodiacal light, the inferred star formation rate, $\sim 0.3 - 15 M_{\odot} \text{ yr}^{-1} \text{ Mpc}^{-3}$ at $z = 7 - 15$ for $m > 5 M_{\odot}$, is significantly higher than the low- z rates. We have shown that this does not exclude the stellar origin of the cosmic near infrared background, as it merely requires more than 0.016{0.59% of baryons to be processed in stars at any given time between $z = 7$ and 15 (depending on metallicity and initial mass

spectrum ; see Table 3). Such a high star formation rate at high z may be consistent with recent theoretical proposals (Cen 2003; Maddey, Bromm, & Hernquist 2003). More accurate determination of the near infrared background is absolutely necessary to yield a meaningful estimate of the star formation rate with any confidence.

We thank K. Ahn, M. Alvarez, V. Bromm, N. J. Evans II, A. Ferrara, J. Scalo, P.R. Shapiro and N. Yoshida for valuable comments on early versions of the paper and fruitful discussions.

A. DERIVATION OF VOLUME EMISSIVITY

In this Appendix we derive the formula for volume emissivity, $p(\epsilon; z)$, which is formally given by

$$p(\epsilon; z) = \int_{m_1}^{m_2} dm \frac{dn(m; z)}{dm} \bar{L}(m); \quad (A1)$$

where ϵ labels various radiative processes (e.g., line), \bar{L} is a time-averaged energy spectrum of relevant emission (luminosity in frequency interval $[\nu, \nu + d\nu]$), and $dn = dm$ is the comoving number density of stars that are alive at a given z in mass interval $[m, m + dm]$. Subtlety exists as we need to properly take into account dead stars. (Since dead stars do not contribute to the emissivity, they must be removed from Eq. [A1].) The goal of this Appendix is to derive the formula for $p(\epsilon; z)$ which is properly corrected for dead stars.

A.1. Case with No Dead Stars

First, as the simplest example (and for illustration purposes) let us derive the formula which does not correct for dead stars. (Note that we do not use this formula. The correct formula will be given in the next subsection.) We write $dn = dm$ as

$$\frac{dn(m; z)}{dm} = n(z)f(m); \quad (A2)$$

where $f(m)$ is a probability distribution function of stellar masses (also known as the mass spectrum) normalized to unity for a certain mass range such that

$$\int_{m_1}^{m_2} dm f(m) = 1; \quad (A3)$$

We assume that $f(m)$ is independent of time. For example, $f(m) \propto m^{-2.35}$, the Salpeter mass spectrum, is independent of time. In principle, however, $f(m)$ may depend on time

when there is a characteristic stellar mass scale (e.g., Larson's mass spectrum) that increases or decreases with time. One may expect m_c to decrease as the metal enrichment proceeds, for example. Nevertheless, we shall assume that m_c is independent of time, at least for the redshift range that we consider.

We may use the comoving mass density of stars, $\rho(z)$, instead of the comoving number density, $n(z)$. The relation is

$$\rho(z) = m \cdot n(z); \quad (\text{A } 4)$$

where m is the mean stellar mass given by

$$m = \frac{\int_{m_1}^{m_2} dm \cdot m f(m)}{\int_{m_1}^{m_2} dm f(m)}; \quad (\text{A } 5)$$

Using this, the volume emissivity (not corrected for dead stars) becomes

$$\rho(\rho; z) = \frac{\int_{m_1}^{m_2} dm f(m) \overline{L}(m)}{\int_{m_1}^{m_2} dm f(m)}; \quad (\text{A } 6)$$

Salvaterra & Ferrara (2003) used a version of this equation⁹, and therefore they did not correct their emissivity for dead stars.

A 2. Emissivity Corrected for Dead Stars

Now, we correct emissivity for dead stars by simply removing them from $n(z)$:

$$\frac{dn(m; z)}{dm} = f(m) \frac{\int_{T_0(z)}^{T_0(z)} dt \underline{n}}{\int_{T_0(z)}^{T_0(z)} dt(m)}; \quad (\text{A } 7)$$

where \underline{n} is a rate of star formation, $T_0(z)$ is the time between when the universe started forming stars and the time corresponding to z , and $\underline{n}(m)$ is a stellar main-sequence lifetime. Equation (A 1) then becomes

$$\rho(\rho; z) = \frac{\int_{m_1}^{m_2} dm f(m) \overline{L}(m)}{\int_{T_0(z)}^{T_0(z)} dt(m)} \frac{dt}{m}; \quad (\text{A } 8)$$

This result may be simplified when the stellar lifetime is much shorter than $T_0(z)$ (which is about the same as the age of the universe at z). As we have shown in Figure 1, the main-sequence lifetime of stars contributing to the near infrared background is always shorter than

⁹ Salvaterra & Ferrara (2003) actually used $\rho(\rho; z) = \int_{m_1}^{\rho} dm f(m) \overline{L}(m) = m$, which is off by a factor of $m = m$.

the age of the universe. We Taylor expand the integral over time to obtain the final formula:

$$p(z) \propto \frac{H(z)}{m} \int_{m_1}^{m_2} dm \, f(m) \bar{L}(m) \, (m) : \quad (A9)$$

B . STELLAR MASS DENSITY

B.1. Case with Dead Stars

Cumulative mass density of stars that were formed at $t_1 < t < t_2$ is given by

$$\text{cum}(t_1; t_2) = \int_{t_1}^{t_2} dt \, \frac{dt}{dt} (t_2 - t) ; \quad (B1)$$

where we have assumed that $\frac{dt}{dt}$ is approximately constant over $t_1 < t < t_2$. Using z instead of t , one gets

$$\begin{aligned} \text{cum}(z_1; z_2) &= \frac{\int_{z_1}^{z_2} dz}{H(z)(1+z)} \\ &= \frac{1}{\int_{z_1}^{z_2} dz} \frac{dz}{(1+z)^{5/2}} \\ &= \frac{5.509}{10^8 M \, M \, pc^3} \frac{10}{(1+z_1)^{3/2}} \frac{10}{(1+z_2)^{3/2}} ; \end{aligned} \quad (B2)$$

where we have assumed that $z_1 = (m)^{1/3} = 1 / 0.3$ so that dark energy contribution to $H(z)$ can be ignored. This is cumulative density, as it includes those stars which had already died. The fractional stellar mass density relative to the critical density, ρ_c , is then given by

$$\begin{aligned} \text{cum}(z_1; z_2) &= \frac{(z_1; z_2)}{c_0} \\ &= \frac{1.985}{10^3} \frac{10}{(1+z_1)^{3/2}} \frac{10}{(1+z_2)^{3/2}} ; \end{aligned} \quad (B3)$$

$$\begin{aligned} \text{cum}(z_1; z_2) h^2 &= \frac{0.14}{m \, h^2} \frac{10}{(1+z_1)^{3/2}} \frac{10}{(1+z_2)^{3/2}} ; \end{aligned} \quad (B4)$$

where $c_0 = 2.775 h^2 \times 10^1 M \, M \, pc^3$ is the present-day critical density.

B 2. Stellar Mass Density Corrected for Dead Stars

We remove dead stars (whose lifetime, $\langle m \rangle$, is much shorter than the Hubble time) from the stellar mass density to obtain

$$(t_1; t_2) = \frac{\int_{m_1}^{m_2} dm f(m) \langle m \rangle}{\int_{m_1}^{m_2} dm f(m)}; \quad (B 5)$$

Comparing this with the cumulative stellar density (Eq. [B 1]), one finds the relation

$$(t_1; t_2) = \frac{\text{cum}(t_1; t_2)}{N_{\text{gen}}}; \quad (B 6)$$

where N_{gen} is the average number of generation of stars:

$$N_{\text{gen}} = \frac{\int_{m_1}^{m_2} dm f(m) t}{\int_{m_1}^{m_2} dm f(m)}; \quad (B 7)$$

C . ANALYTICAL MODEL OF THE COSMIC STAR FORMATION RATE

A popular assumption usually made for an analytical model of the cosmic star formation rate at high z is that $\langle z \rangle$ is related to the mass function of dark matter halos:

$$\langle z \rangle = \bar{\rho}_{b0} H(z) (1+z) \frac{\partial F[M > M_{\text{min}}(z)]}{\partial z}; \quad (C 1)$$

where $\bar{\rho}_{b0} = 2.775 \times 10^1 (\Omega_b h^2) \text{ Mpc}^{-3}$ is the present-day mean baryon density, and represents a "star formation efficiency", a constant fraction of baryonic gas in dark matter halos that was converted into stars. It is admittedly too simplistic to assume that $\langle z \rangle$ is independent of halo mass or redshift. For example, negative feedback from a star forming in a single mini-halo might prevent the formation of multiple stars in the same halo, which would imply $\langle z \rangle / M^{-1}$. Therefore, this parameterization of the efficiency serves merely as an order-of-magnitude representation of the true efficiency. Finally, F is a "collapse fraction", a fraction of mass in the universe collapsed into halos more massive than $M_{\text{min}}(z)$,

$$F[M > M_{\text{min}}(z)] = \frac{1}{\bar{\rho}_m M_0} \int_{M_{\text{min}}(z)}^{Z_1} dM \frac{dn_h(M; z)}{dM} M; \quad (C 2)$$

where $\bar{\rho}_m = 2.775 \times 10^1 (\Omega_m h^2) \text{ Mpc}^{-3}$ is the present-day mean total mass density, and M is the halo mass (not to be confused with the stellar mass, m), and dn_h/dM is the halo mass function. The Press-Schechter mass function gives the collapse fraction in terms of the complementary error function,

$$F[M > M_{\text{min}}(z)] = \frac{1}{2} \int_{y_{\text{min}}(z)}^{Z_1} dy e^{-y^2/2}; \quad (C 3)$$

where

$$Y_{\text{min}}(z) = \frac{c}{M_{\text{min}}(z)D(z)} = \frac{1.68(1+z)}{M_{\text{min}}(z)}; \quad (\text{C } 4)$$

in the redshift range of interest ($z > 7$). One thus finds

$$\begin{aligned} \frac{\partial F[M > M_{\text{min}}(z)]}{\partial z} &= \frac{r}{2} \frac{dy_{\text{min}}}{dz} e^{y_{\text{min}}^2/2} \\ &\quad \# \\ &\quad \frac{2}{1+z} \frac{Y_{\text{min}}(z)}{1+z} + \frac{d \ln M_{\text{min}}(z)}{d \ln(1+z)} \frac{d \ln}{d \ln M} \frac{1}{M = M_{\text{min}}(z)} e^{y_{\text{min}}^2/2} \\ &= \frac{2}{1+z} \frac{Y_{\text{min}}(z)}{1+z} \frac{1 - n_e[M_{\text{min}}(z)]}{4} e^{y_{\text{min}}^2/2}; \end{aligned} \quad (\text{C } 5)$$

Here, we have assumed that $M_{\text{min}}(z)$ is proportional to the virial mass and thus $M_{\text{min}}(z) / (1+z)^{2/3}$, and defined an effective slope of the power spectrum as $n_e(M) + 3/6 = d \ln^{-1} = d \ln M$. At the scale of interest, the effective slope lies between 2.5 and 2.8; thus, the prefactor, $(1 - n_e) = 4$, is of order unity and the exact value is not so important. Setting it to be unity, we obtain a fully analytical formula for the star formation rate at high redshifts,

$$\begin{aligned} \dot{\rho}(z) &= \frac{r}{2} \frac{1}{b_0} H(z) Y_{\text{min}}(z) e^{y_{\text{min}}^2/2} \\ &= 0.536 M_{\text{pc}}^{-3} \text{yr}^{-1} \frac{b_0 h^2}{0.1 \cdot 0.02} \frac{m h^2}{0.14}^{1/2} \\ &\quad \frac{1+z}{10}^{3/2} Y_{\text{min}}(z) e^{y_{\text{min}}^2/2}; \end{aligned} \quad (\text{C } 6)$$

REFERENCES

Barkana, R., & Loeb, A. 2001, *Phys. Rep.*, 349, 125

Becker, R. H. 2001, *AJ*, 122, 2850

Boggess, N. W., et al. 1992, *ApJ*, 397, 420

Bromm, V., & Larson, R. B. 2004, *ARA & A*, 42, 79

Bromm, V., Kudritzki, R. P., & Loeb, A. 2001, *ApJ*, 552, 464

Brown, R. L., & Matthews, W. G. 1970, *ApJ*, 160, 939

Cambresy, L., Reach, W. T., Beichman, C. A., & Jarrett, T. H. 2001, *ApJ*, 555, 563

Cen, R. 2003, *ApJ*, 591, 12

Ciardi, B., & Ferrara, A. 2005, *Space Science Reviews*, 116, 625

Ciardi, B., & Madau, P. 2003, *ApJ*, 596, 1

Cooray, A., & Yoshida, N. 2004, *MNRAS*, 351, L71

Cooray, A., Bock, J. J., Keating, B., Lange, A. E., & Matsumoto, T. 2004, *ApJ*, 606, 611

Dopita, M. A., & Sutherland, R. S. 2002, *Astrophysics of the diffuse Universe* (Springer)

Dory, N., Salvato, M., Gabasch, A., Bender, R., Hopp, U., Feulner, G., & Pannella, M. 2005, *ApJ*, 619, L131

Dwek, E., & Arendt, R. G. 1998, *ApJ*, 508, L9

Furlanetto, S. R., Sokasian, A., & Hernquist, L. 2004, *ApJ*, 347, 187

Gabasch, A., et al. 2004, *A&A*, 4211, 41

Orján, V., Wright, E. L., & Chary, R. R. 2000, *ApJ*, 536, 550

Gunn, J. E., & Peterson, B. A. 1965, *ApJ*, 142, 1633

Hui, L., & Haiman, Z. 2003, *ApJ*, 596, 9

Iliev, I. T., Shapiro, P. R., Ferrara, A., & Martel, H. 2002, *ApJ*, 572, L123

Kaplinghat, M., Chu, M., Haiman, Z., Holder, G. P., Knox, L., & Skordis, C. 2003, *ApJ*, 583, 24

Kashlinsky, A., & Odenwald, S. 2000, *ApJ*, 528, 74

Kashlinsky, A., Odenwald, S., Mather, J. C., Skrutskie, M. F., & Cutri, R. M. 2000, *ApJ*, 579, L53

Kashlinsky, A., Arendt, R., Gardner, J. P., Mather, J. C., & Moseley, S. H. 2004, *ApJ*, 608, 1

Karzas, W. J., & Latter, R. 1961, *ApJS*, 6, 167

Kogut, A., et al. 2003, *ApJS*, 148, 161

Larson, R. B. 1999, *MNRAS*, 301, 569

Loeb, A., & Rybicki, G. B. 1999, *ApJ*, 524, 527

Mackey, J., Bromm, V., & Hernquist, L. 2003, *ApJ*, 586, 1

Madau, P., & Silk, J. 2005, *MNRAS*, 359, L22

Madau, P., Meiksin, A., & Rees, M. J. 1997, *ApJ*, 475, 429

Magliocchetti, M., Salvaterra, R., & Ferrara, A. 2003, *MNRAS*, 342, L25

Matsumoto, T., et al. 2005, *ApJ*, 626, 31 (2005)

Peacock, J. A. 1999, *Cosmological Physics* (Cambridge University Press), pp 91–94

Press, W. H., & Schechter, P. 1974, *ApJ*, 187, 425

Salpeter, E. E. 1955, *ApJ*, 121, 161

Salvaterra, R., & Ferrara, A. 2003, *MNRAS*, 339, 973

Santos, M. R., Bromm, V., & Kamionkowski, M. 2002, *MNRAS*, 336, 1082

Scott, D., & Rees, M. J. 1990, *MNRAS*, 247, 510

Schaller, G., Schaerer, D., Meynet, G., & Maeder, A. 1992, *A&A*, 96, 269

Schaerer, D. 2002, *A&A*, 382, 28

Shapiro, P. R., & Girioux, M. L. 1987, *ApJ*, 321, L107

Spitzer, L. 1978, *Physical Processes in the Interstellar Medium* (John Wiley & Sons)

Tozzi, P., Madau, P., Meiksin, A., & Rees, M. J. 2000, *ApJ*, 528, 597

Tumlinson, J., & Shull, J. M. 2000, *ApJ*, 528, L65

Wright, E. L. 2001, *ApJ*, 553, 538

Wright, E. L., & Reese, E. D. 2000, *ApJ*, 545, 43

Zaldarriaga, M. 1997, *Phys. Rev. D*, 55, 1822